9-14-2012

Polarization-Induced Hysteresis in CuCo-Doped Rare Earth Vanadates SOFC Anodes

Lawrence Adijanto
University of Pennsylvania

Venu Balaji Padmanabhan
University of Pennsylvania

Raymond J. Gorte
University of Pennsylvania, gorte@seas.upenn.edu

John M. Vohs
University of Pennsylvania, vohs@seas.upenn.edu

Follow this and additional works at: http://repository.upenn.edu/cbe_papers

Part of the Chemical Engineering Commons

Recommended Citation

Adijanto, L., Padmanabhan, V., Gorte, R. J., & Vohs, J. M. (2012). Polarization-Induced Hysteresis in CuCo-Doped Rare Earth Vanadates SOFC Anodes. Retrieved from http://repository.upenn.edu/cbe_papers/158

Polarization-Induced Hysteresis in CuCo-Doped Rare Earth Vanadates SOFC Anodes

Abstract

The physical and electrochemical properties of strontium substituted cerium vandates in which a portion of the cerium cations have been substituted with transition metals ($Ce_{0.8}Sr_{0.1}Cu_{0.05}TM_{0.05}VO_{4-0.5x}$, TM = Ni or Co) were investigated and their suitability for use in solid oxide fuel cell (SOFC) anodes was assessed. Upon reduction at elevated temperature, Cu and Co or Cu and Ni were exsolved from the electronically conductive $Ce_{1-x}Sr_xVO_4$ lattice to produce Cu-Ni and Cu-Co catalytic nanoparticles. The $Ce_{0.8}Sr_{0.1}Cu_{0.05}Co_{0.05}VO_3$ appears to have high activity and relatively high hydrocarbon tolerance, suggesting that intimate contact between the exsolved Cu and Co and that the majority of the Co nanoparticles must be at least partially coated with the Cu. The electrochemical performance when used in anodes operating on hydrogen has been characterized, and the results demonstrate the exsolution of both metals from the host lattice; but observed dynamic changes in the structure of the resulting metal nanoparticles as a function of SOFC operating conditions complicate their use in SOFC anodes.

Disciplines
Chemical Engineering

Polarization-Induced Hysteresis in CuCo-Doped Rare Earth Vanadates SOFC Anodes

Lawrence Adijanto,* **Venu Balaji Padmanabhan, Raymond J. Gorte,** **and John M. Vohs****,z

Department of Chemical and Biomolecular Engineering, University of Pennsylvania, Philadelphia, Pennsylvania 19104-6315, USA

The physical and electrochemical properties of strontium substituted cerium vandates in which a portion of the cerium cations have been substituted with transition metals ($Ce_{0.8}Sr_{0.1}Cu_{0.05}TM_{0.05}VO_{4-0.5x}$, TM = Ni or Co) were investigated and their suitability for use in solid oxide fuel cell (SOFC) anodes was assessed. Upon reduction at elevated temperature, Cu and Co or Cu and Ni were exsolved from the electronically conductive $Ce_{1-x}Sr_xVO_4$ lattice to produce Cu-Ni and Cu-Co catalytic nanoparticles. The $Ce_{0.8}Sr_{0.1}Cu_{0.05}Co_{0.05}VO_3$ appears to have high activity and relatively high hydrocarbon tolerance, suggesting that intimate contact between the exsolved Cu and Co and that the majority of the Co nanoparticles must be at least partially coated with the Cu. The electrochemical performance when used in anodes operating on hydrogen has been characterized, and the results demonstrate the exsolution of both metals from the host lattice; but observed dynamic changes in the structure of the resulting metal nanoparticles as a function of SOFC operating conditions complicate their use in SOFC anodes.
© 2012 The Electrochemical Society. [DOI: 10.1149/2.042211jes] All rights reserved.

Solid oxide fuel cells (SOFCs) are of interest due to their relatively high energy conversion efficiencies and fuel flexibility. The fuel flexibility of SOFCs results from the fact that O^{2-} anions, rather than H^+ ions, are transmitted through the electrolyte. Direct utilization of hydrocarbons, however, is still not possible in conventional SOFCs because Ni-YSZ composites, the most commonly used anode composition, catalyze the formation of carbon deposits including fibers that cause deactivation.[1–5] One solution to this problem is to replace the Ni with an electronically conductive material that does not catalyze the formation of carbon from hydrocarbon fuels. Electronically conductive ceramics, including titanates,[6–10] manganates,[11–14] chromates,[15] and bronzes[16,17] have been investigated for this application. These materials have been shown to have a low susceptibility to sintering and coking and are more redox stable and tolerant of impurities, like sulfur, than Ni.[5,18–21] While promising results have been obtained with ceramic-based anodes, these anodes unfortunately have relatively low catalytic activity for oxidation reactions, resulting in high electrode overpotentials unless they are decorated with nanoparticles of a highly catalytic metal (e.g. Ni, Pt, or Pd).[2,8,11,15–17,22–29] Sintering of the catalytic nanoparticles, however, is still an issue that hinders the long-term stability of the anode.

One approach that has been proposed to enhance the catalytic activity of ceramic-based anodes is to use materials for which the metal nanoparticle catalysts can be generated in situ through their exsolution from a conducting perovskite host.[11,15,23,29–37] This concept is similar to that used in self-regenerating automotive emissions catalysts that were first developed by researchers at Daihatsu.[33,35–37] So called "intelligent" automotive catalysts use perovskite (ABO_3) oxides (e.g. $LaFeO_3$) in which a catalytic metal, typically the noble metals Pd, Pt or Rh, is substituted for a small portion of the B-site cations. Under mildly reducing conditions the easily reduced noble metal cations are exsolved from the lattice and precipitate as nanoparticles that decorate the surface of the perovskite. Since the catalytic converter in an automotive emissions control system oscillates between oxidizing and reducing conditions, the noble metals undergo dissolution/exsolution cycles that help maintain the metal surface area and catalytic activity. The Barnett group has recently demonstrated the use of this phenomenon in SOFC anodes.[15,23,28,31] They used the electronically conducting perovskite, $La_{0.8}Sr_{0.2}Cr_{1-x}M_xO_{3-x}$ where M = Ni, Pd, and Ru, and showed that metal nanoparticles with diameter of <5 nm were produced from the perovskite lattice upon exposure to a reducing environment.[15,23,28,31] This in turn greatly enhanced the performance of electrodes based on this material. Since redox cycling could also be used in an SOFC to regenerate any metal surface area loss due to sintering, this approach provides a novel strategy for both optimizing the catalytic properties of ceramic anodes for SOFC for specific fuels and for maintaining long-term performance.

While exsolution of catalytic metals can be used to enhance the catalytic activity of an SOFC anode, in order to obtain a high performance anode, the host oxide must also have high electronic conductivity. Recently, we and others have shown that alkaline earth (AE) substituted rare earth (RE) vanadates ($RE_{1-x}AE_xVO_4$), such as $Ce_{1-x}Sr_xVO_4$ and $La_{1-x}Sr_xVO_4$, have electronic conductivities approaching 1000 S cm^{-1} under some conditions, and are chemically stable in a variety of fuels including H_2, H_2S, and CH_4.[38–47] These properties make the vanadates ideal candidates for use in SOFC anodes designed to run on hydrocarbon fuels. We have also demonstrated that when doped with catalytic metals, Ni and Co, the metals can be exsolved from the lattice upon exposure to reducing atmospheres.[30] While similar to the perovskites discussed above, the vanadates exhibit a somewhat more complex phase behavior. In their fully oxidized form, $RE_{1-x}AE_xVO_4$ has a zircon structure. Upon exposure to reducing conditions, however, they undergo a phase change to the perovskite structure.[30,40,45] Exsolution of a portion of the metals from the lattice accompanies this phase change.[30]

$RE_{1-x}AE_xVO_4$ anodes doped with Co or Ni (used as a composite with YSZ) have been shown to exhibit high electrochemical activity and unusually high redox stability, with the latter property being partially due to the exsolution/dissolution of the catalytic metals. These anodes, however, are not hydrocarbon stable since both Ni and Co catalyze carbon formation.[30] It has previously been shown in studies of anodes with a more conventional design that the propensity for Ni and Co to catalyze coke deposition can be ameliorated by alloying with a less reactive metal, such as Cu, while still maintaining high oxidation activity.[19,48–53] Particles composed of Ni and Cu, form a solid solution so that both Cu and Ni remain at the surface. Based on previous work, Cu-Ni alloys exposed to dry methane still formed significant amounts of carbon up to alloy compositions of 20% Ni. Unlike Cu-Ni alloys, the Cu and Co in Cu-Co mixtures remain as separate phases, with the surface enriched in Cu due to its lower surface free energy. The low activity for C-C bond breaking and forming on Cu causes these particles to have a lower activity for coke formation, even for compositions with high Co:Cu ratios. Enough of the more active metal remains exposed, however, to allow relatively high catalytic activity for oxidation reactions to be maintained.

In the present study we have explored the possibility of doping $RE_{1-x}AE_xVO_4$ with both Cu and Co or Cu and Ni and using the exsolution phenomena described above as an in situ means to synthesize Cu-Ni and Cu-Co catalytic nanoparticles, with the goal of using these materials to produce high-performance, highly robust SOFC

*Electrochemical Society Student Member.
**Electrochemical Society Active Member.
zE-mail: vohs@seas.upenn.edu

anodes that can directly utilize hydrocarbon-based fuels. Specific materials that have been studied include $Ce_{0.8}Sr_{0.1}Cu_{0.05}Co_{0.05}VO_3$ and $Ce_{0.8}Sr_{0.1}Cu_{0.05}Ni_{0.05}VO_3$. The exsolution of the metals from these materials and their electrochemical performance when used in anodes operating on hydrogen have been characterized. Preliminary studies of their hydrocarbon stability are also reported. The results obtained in this study demonstrate the exsolution of both metals from the host lattice, but observed dynamic changes in the structure of the resulting metal nanoparticles as a function of SOFC operating conditions complicate their use in SOFC anodes.

Experimental

Bulk $Ce_{0.8}Sr_{0.1}Cu_{0.05}TM_{0.05}VO_{4-\delta}$ powders were used for XRD analysis and (where TM = Ni, Co) were prepared using an aqueous precursor solution containing the appropriate amounts of $Ce(NO_3)_3.6H_2O$ (Alfa Aesar, 99.5%), $Sr(NO_3)_2$ (Alfa Aesar, 99.9%), NH_4VO_3 (Aldrich, 99+%), and either $Ni(NO_3)_2.6H_2O$, $Co(NO_3)_2.6H_2O$, or $Cu(NO_3)_2.3H_2O$ (Alfa Aesar, 99.9%). Citric acid (Fisher Scientific) was also added as a complexing agent to aid in the formation of a more homogeneous mixture. The precursor solution was dried and the resulting powder was calcined at 973 K in air to form the zircon phase. Perovskite $Ce_{0.8}Sr_{0.1}Cu_{0.05}TM_{0.05}VO_3$ materials were produced by reducing the $Ce_{0.8}Sr_{0.1}Cu_{0.05}TM_{0.05}VO_{4-\delta}$ in humidified H_2 (3% H_2O) at 973 K.

Porous YSZ slabs into which 30 wt% $Ce_{0.8}Sr_{0.1}Cu_{0.05}TM_{0.05}VO_{4-\delta}$ had been infiltrated were used for hydrocarbon stability measurements. The porous, 4 mm × 4 mm × 15 mm YSZ slabs were prepared using methods that have been described in detail previously.[54,55] The vanadates were added to the porous YSZ slabs by infiltrating the aqueous precursor solution followed by drying and annealing in air at 973 K. Multiple infiltration/annealing cycles were used to obtain the desired 30 wt% loading. The stability of the vanadates in hydrocarbons was assessed by exposing $Ce_{0.8}Sr_{0.1}Cu_{0.05}TM_{0.05}VO_3$/YSZ composites under humidified H_2 (3% H_2O) for 3 hours at 1073 K before exposing them to dry methane at 1073 K for 3 hours and measuring their weight gain resulting from carbon deposition. The morphological structure of the porous composites was determined using scanning electron microscopy (SEM) (FEI Quanta 600 ESEM) and X-ray diffraction (XRD) using Cu K_α radiation. For the XRD measurements, a small amount of YSZ was physically mixed with the oxides to act as a reference.

Solid oxide fuel cells 1-cm in diameter were used in all fuel cell measurements. These cells were fabricated using porous-dense-porous tri-layer YSZ wafers that were produced using tape casting methods that have been described in detail previously.[54] For each cell, the dense electrolyte layer was 65-μm thick and 1-cm in diameter. The 60% porous YSZ layers on each side of the dense electrolyte layer were 50-μm thick with a BET surface area 0.3 m^2g^{-1}. 40 wt% Sr-doped lanthanum ferrite, $La_{0.8}Sr_{0.2}FeO_3$ (LSF), was added to one porous layer to form a cathode using multiple cycles of infiltration of an aqueous solution containing dissolved $La(NO_3)_3.6H_2O$ (Alfa Aesar, 99.9%), $Sr(NO_3)_2$ (Alfa Aesar, 99%) and $Fe(NO_3)_3.9H_2O$ (Fisher Scientific) in the appropriate molar ratios, followed by calcination in air at 723 K.[56–58] After the infiltration steps the composite cathode was calcined to 1123 K for 4 h to form the perovskite structure. Previous studies have shown that cathodes of this design have an ASR of $\sim$0.15 Ω cm^2 in air at 973 K.[16,58] The $Ce_{0.8}Sr_{0.1}Cu_{0.05}TM_{0.05}VO_3$ anode was synthesized in a similar manner except that a 30 wt% loading was used and it was calcined to only 973 K. The anode was reduced in humidified H_2 (3% H_2O) at 973 K prior to cell testing. Silver paste current collectors were applied to both electrodes and the cells were mounted onto an alumina tube using a ceramic adhesive (Aremco, Ceramabond 552). All the cell tests were performed with the cathode exposed to ambient air and the anode exposed to humidified H_2. Electrochemical impedance spectra were measured between 0.1 Hz and 300 kHz with a 1 mA AC perturbation. Both impedance spectra and V-i polarization curves were measured using a Gamry Instruments potentiostat.
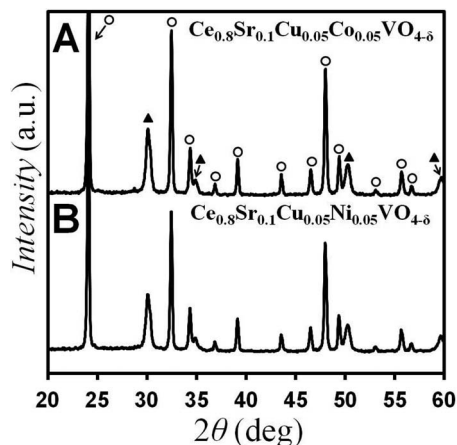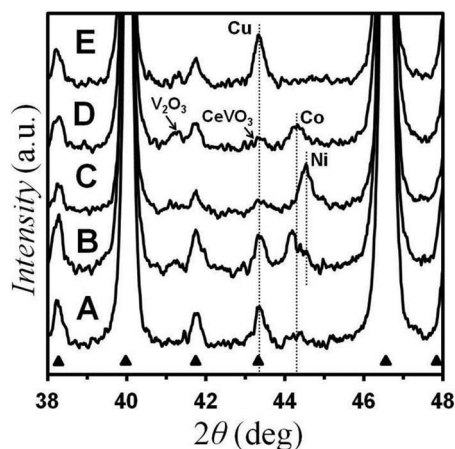

Figure 1. XRD patterns of (A) $Ce_{0.8}Sr_{0.1}Cu_{0.05}Co_{0.05}VO_{4-\delta}$, and (B) $Ce_{0.8}Sr_{0.1}Cu_{0.05}Ni_{0.05}VO_{4-\delta}$ oxidized at 973 K in air. The peaks are labeled as follows: (▲) cubic YSZ, (○) zircon $Ce_{0.8}Sr_{0.1}Cu_{0.05}Co_{0.05}VO_{4-\delta}$ and $Ce_{0.8}Sr_{0.1}Cu_{0.05}Ni_{0.05}VO_{4-\delta}$.

Results and Discussion

XRD was used to determine the phase composition of the Cu and Co or Cu and Ni vanadates following various pretreatments. XRD patterns for (A) $Ce_{0.8}Sr_{0.1}Cu_{0.05}Co_{0.05}VO_{4-\delta}$ and (B) $Ce_{0.8}Sr_{0.1}Cu_{0.05}Ni_{0.05}VO_{4-\delta}$ samples that were calcined in air at 973 K for 2 hrs are presented in Figure 1. The zircon structure of $Ce_{0.8}Sr_{0.1}Cu_{0.05}Co_{0.05}VO_{4-\delta}$ and $Ce_{0.8}Sr_{0.1}Cu_{0.05}Ni_{0.05}VO_{4-\delta}$ was confirmed by the presence of the expected diffraction peaks near 24.0, 32.4, 34.1, 36.4, 38.9, 43.2, 46.1, and 48.0 degrees 2θ.[43,46] The XRD patterns are comprised of peaks that correspond only to $Ce_{0.8}Sr_{0.1}Cu_{0.05}Co_{0.05}VO_{4-\delta}$ and $Ce_{0.8}Sr_{0.1}Cu_{0.05}Ni_{0.05}VO_{4nm\delta}$ and do not contain any peaks indicative of other oxide phases including $TM_2V_2O_7$ (where TM = Ni, Co, or Cu), thus demonstrating that the single phase vanadates were formed.

As noted above, the transition metal doped vanadates undergo a phase change from the zircon structure to the perovskite structure upon reduction, with a portion of the metals being exsolved from the lattice.[30] This is demonstrated by the XRD patterns in Figure 2 for (A) $Ce_{0.8}Sr_{0.1}Cu_{0.05}Co_{0.05}VO_3$ and (B) $Ce_{0.8}Sr_{0.1}Cu_{0.05}Ni_{0.05}VO_3$ samples that were reduced in humidified H_2 at 973 K. For comparison purposes, XRD patterns for reduced vanadates that contain only one of

Figure 2. XRD patterns of (A) $Ce_{0.8}Sr_{0.1}Cu_{0.05}Co_{0.05}VO_3$, (B) $Ce_{0.8}Sr_{0.1}Cu_{0.05}Ni_{0.05}VO_3$, (C) $Ce_{0.8}Sr_{0.1}Ni_{0.1}VO_3$, (D) $Ce_{0.8}Sr_{0.1}Co_{0.1}VO_3$, and (E) $Ce_{0.8}Sr_{0.1}Cu_{0.1}VO_3$ reduced under humidified H_2 at 973 K. The dotted lines indicate the position of the Ni, Co, and Cu metal peaks. The (▲) peaks correspond to Sr doped-$CeVO_3$.

the transition metals ((C) $Ce_{0.8}Sr_{0.1}Ni_{0.1}VO_3$, (D) $Ce_{0.8}Sr_{0.1}Co_{0.1}VO_3$, and (E) $Ce_{0.8}Sr_{0.1}Cu_{0.1}VO_3$) are also included in the figure. The large peaks at 40.1 and 46.7 degrees 2θ are indicative of the perovskite phase. Peaks corresponding to the bulk transition metals are also apparent between 43 and 45 degrees 2θ for each sample. The positions of the expected peak for each metal are indicated in the figure. Note that the Cu diffraction peak overlaps with one of the minor peaks for the perovskite vanadate. The presence of peaks indicative of the transition metals in each pattern further demonstrates that the phase transition from zircon to perovskite is accompanied by the exsolution of the transition metals from the lattice.

Note that the XRD pattern for $Ce_{0.8}Sr_{0.1}Cu_{0.05}Co_{0.05}VO_3$ (pattern A) contains peaks indicative of both Cu and Co, thereby demonstrating that both metals have been exsolved form the host oxide lattice upon reduction. Similarly, the pattern for $Ce_{0.8}Sr_{0.1}Cu_{0.05}Ni_{0.05}VO_3$ (pattern B) contains peaks for both Cu and Ni. For this sample an additional peak is also present at 44.2 degrees 2θ. Unlike Cu and Co, Cu and Ni are miscible.[49,52,53] We therefore assign the peak at 44.2 degrees 2θ to the formation of Cu-Ni alloy particles. Although particles with a range of compositions are likely to have been formed, the 44.2 degrees 2θ peak position is consistent with a 50:50 Cu:Ni alloy composition.[53]

While the exsolved metals would be expected to enhance the catalytic activity of an SOFC anode made with these materials, as discussed in the introduction, intimate contact between the Cu and the Co or Ni will be required to produce catalysts that do not undergo severe coking upon exposure to hydrocarbons. To assess whether this can be achieved for transition metal decorated surfaces produced by reduction of $Ce_{0.8}Sr_{0.1}Cu_{0.05}Co_{0.05}VO_3$ and $Ce_{0.8}Sr_{0.1}Cu_{0.05}Ni_{0.05}VO_3$, we exposed porous composites of these materials with YSZ to dry methane at 1073 K for 3 hrs. SEM images of these samples after this treatment are displayed in Figure 3. For comparison purposes, images obtained from reduced $Ce_{0.8}Sr_{0.1}Cu_{0.1}VO_3$-YSZ and $Ce_{0.8}Sr_{0.1}Co_{0.1}VO_3$-YSZ composites subjected to the same treatment are also include in the figure. The weight gain for each sample after the hydrocarbon treatment is listed in Table I.

Panel A in Figure 3 corresponds to the CH_4-treated $Ce_{0.8}Sr_{0.1}Cu_{0.1}VO_3$-YSZ composite. Cu is a relatively unreactive metal and does not catalyze carbon fiber formation from hydrocarbons.[30,53] As expected, this image does not contain any evidence for carbon deposition, and this sample exhibited only a negligible weight gain. In contrast, for the reduced $Ce_{0.8}Sr_{0.1}Co_{0.1}VO_3$-YSZ sample whose surfaces are decorated with Co nanoparticles, worm-like carbon fibers are readily apparent in the SEM image obtained after

Table I. Percentage weight changes after exposure to dry CH_4 at 1073 K for 3 hrs.

Sample	% weight gain
$Ce_{0.8}Sr_{0.1}Cu_{0.1}VO_3$	< 1
$Ce_{0.8}Sr_{0.1}Co_{0.1}VO_3$	12
$Ce_{0.8}Sr_{0.1}Cu_{0.05}Co_{0.05}VO_3$	2
$Ce_{0.8}Sr_{0.1}Cu_{0.05}Ni_{0.05}VO_3$	61

exposure to CH_4 (panel B, Fig. 3) and this sample exhibited a 12% weight gain. Unfortunately, similar results were obtained from the $Ce_{0.8}Sr_{0.1}Cu_{0.05}Ni_{0.05}VO_3$-YSZ composite. The SEM image for this sample (panel C, Fig. 3) shows the presence of a high concentration of carbon fibers and the weight of the sample increased by 61%. The high activity of this sample for carbon fiber formation is consistent with previous results for Cu-Ni alloys.[19] Although one would expect some suppression of the carbon formation in Cu-Ni alloys, carbon formation with a 50:50 Cu-Ni alloy is still significant. More promising results were obtained for the $Ce_{0.8}Sr_{0.1}Cu_{0.05}Co_{0.05}VO_3$-YSZ composite. The SEM image of this sample after exposure to CH_4 (panel D, Fig. 3) is nearly devoid of carbon fibers and the weight gain for the sample was only 2%. Since Co is highly active for carbon fiber formation, this result indicates that there is intimate contact between the exsolved Cu and Co and that the majority of the Co nanoparticles must be at least partially coated with the Cu.

Based on the hydrocarbon stability tests, the Cu-Co substituted vanadates were considered more promising for use in SOFC anodes and were therefore the focus of electrochemical testing. This was done using SOFC button cells that with a 65-μm thick YSZ electrolyte, an infiltrated 30 wt% $Ce_{0.8}Sr_{0.1}Cu_{0.05}Co_{0.05}VO_3$-YSZ composite anode, and a 40 wt% LSF-YSZ composite cathode.[56–58] For comparison purposes, cells with $Ce_{0.8}Sr_{0.1}Cu_{0.1}VO_3$-YSZ, $Ce_{0.8}Sr_{0.1}Co_{0.1}VO_3$-YSZ, and $CeVO_3$-YSZ composite anodes were also used in some experiments. The fuel-cell measurements reported here focused on characterizing stability of the $Ce_{0.8}Sr_{0.1}Cu_{0.05}Co_{0.05}VO_3$-YSZ anode while operating with humidified H_2 (3% H_2O) fuel.

Polarization curves for each cell at 973 K using humidified H_2 as fuel are shown in Figure 4. Each curve was measured starting from OCV, followed by ramping the potential to 0 V and back to OCV using a linear scan rate of 0.025 Vs^{-1} in both directions. The polarization curves for the cells with the $CeVO_3$-YSZ (dashed black curve) and $Ce_{0.8}Sr_{0.1}Cu_{0.1}VO_3$-YSZ (dashed blue curve) and $Ce_{0.8}Sr_{0.1}Co_{0.1}VO_3$-YSZ (dotted red curve) were all nearly linear and reversible, showing the same behavior in both scan directions. As will be discussed below, more complex hysteretic behavior was observed for the cell with the

Figure 3. SEM images of the (A) $Ce_{0.8}Sr_{0.1}Cu_{0.1}VO_3$-, (B) $Ce_{0.8}Sr_{0.1}Co_{0.1}VO_3$-, (C) $Ce_{0.8}Sr_{0.1}Cu_{0.05}Ni_{0.05}VO_3$-, (D) $Ce_{0.8}Sr_{0.1}Cu_{0.05}Co_{0.05}VO_3$-YSZ composites that had been exposed to dry methane at 1073 K for 3 hrs.
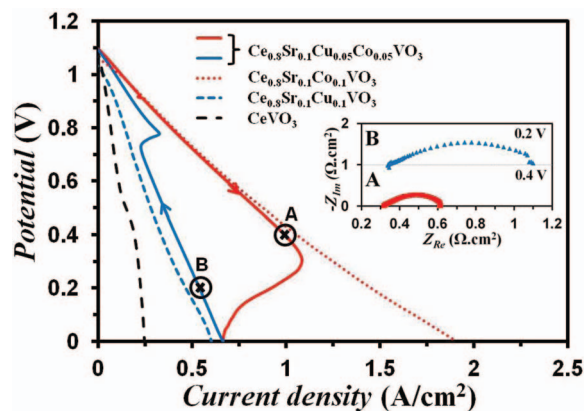

Figure 4. V-i polarization curves for cells with infiltrated 30 wt% of (—,—) $Ce_{0.8}Sr_{0.1}Cu_{0.05}Co_{0.05}VO_3$, (--) $Ce_{0.8}Sr_{0.1}Co_{0.1}VO_3$, (−−) $Ce_{0.8}Sr_{0.1}Cu_{0.1}VO_3$, and (——) $CeVO_3$ –YSZ anodes. Inset: Electrochemical impedance spectra of $Ce_{0.8}Sr_{0.1}Cu_{0.05}Co_{0.05}VO_3$ cell measured at (A) 0.4 V and (B) 0.2 V. The cells were operated at 973 K with humidified H_2 fuel.

$Ce_{0.8}Sr_{0.1}Cu_{0.05}Co_{0.05}VO_3$-YSZ anode. Each cell had an open-circuit potential near the theoretical Nernst value of 1.1 V. As reported previously, relatively poor electrochemical performance was obtained from the cell with the $CeVO_3$-YSZ composite anode (ASR_{anode} = 2.70 Ω cm^2) due to the low catalytic activity of this material.[30,47] Only slightly better performance was obtained for the cell with the $Ce_{0.8}Sr_{0.1}Cu_{0.1}VO_3$-YSZ anode ($ASR_{anode}$ = 0.65 Ω cm^2) which is consistent with the low catalytic activity of both Cu and the vanadate. Excellent performance was obtained from the cell with the $Ce_{0.8}Sr_{0.1}Co_{0.1}VO_3$-YSZ anode which had an ASR_{anode} of only 0.1 Ω cm^2 (This assumes that the cathode ASR 0.15 Ω cm^2, as determined in other work.[16,58]). This result is consistent with the surface of the $Ce_{0.8}Sr_{0.1}Co_{0.1}VO_3$ being decorated with highly catalytic Co nanoparticles under reducing conditions as demonstrated above.

Unusually complex behavior was exhibited by the cell with the $Ce_{0.8}Sr_{0.1}Cu_{0.05}Co_{0.05}VO_3$-YSZ composite anode, including hysteresis in the polarization curve, with abrupt changes in performance occurring at several voltages (Figure 4). The initial portion of the polarization curve for this cell, starting from OCV and ramping to ~0.3 V (solid red curve in Fig. 4), closely follows that of the cell with the $Ce_{0.8}Sr_{0.1}Co_{0.1}VO_3$-YSZ anode. As shown by the impedance spectrum obtained at point A (see figure insert), the anode ASR in this portion of the polarization curve is 0.15 Ω cm^2 after subtracting off the cathode ASR, 0.15 Ω cm^2. The hydrocarbon stability tests described above indicated that the Co nanoparticles exsolved from the $Ce_{0.8}Sr_{0.1}Cu_{0.05}Co_{0.05}VO_3$ lattice under reducing conditions are primarily coated with Cu. The similarity in the initial performance of the two anode formulations containing Co, however, demonstrates that, for the $Ce_{0.8}Sr_{0.1}Cu_{0.05}Co_{0.05}VO_3$-YSZ anode, enough Co remains exposed to impart high catalytic activity for H$_2$ oxidation.

Near 0.3 V, an abrupt change in the electrochemical properties of the $Ce_{0.8}Sr_{0.1}Cu_{0.05}Co_{0.05}VO_3$-YSZ anode takes place, causing a rapid decrease in cell performance as the voltage is ramped from 0.3 to 0 V. As shown by the solid blue curve in Figure 4, the polarization curve for the $Ce_{0.8}Sr_{0.1}Cu_{0.05}Co_{0.05}VO_3$ cell exhibited hysteresis and was not immediately reversible, with low performance persisting upon reversal of the sweep direction from 0 to ~0.78 V. In this region of the polarization curve the cell performance was close to that of the cell with the $Ce_{0.8}Sr_{0.1}Cu_{0.1}VO_3$-YSZ anode. As shown by the impedance spectrum collected at point B, the anode ASR in this region of the polarization curve was 0.65 Ω cm^2 (the estimated cathode ASR of 0.15 Ω cm^2 has again been taken into account here). At 0.78 V on the increasing voltage sweep, another abrupt change occurs, with the cell performance switching from the low-activity state back to the high-activity state exhibited by the fresh cell. This high-activity state then persists up to OCV. The hysteretic behavior exhibited by this cell was stable and occurred for repeated polarization curve measurements at a variety of scan rates. Similar results were obtained with multiple cells and the changes in performance occurred at nearly the same voltages (~0.3 and ~0. 8 V) in all cases.

It is important to note that the impedance spectra show that the ohmic contribution remained fixed at 0.3 Ω cm^2 in both the high- and low-performance regions of the polarization curve. This value is consistent with that expected for the 65 μm thick YSZ electrolyte layer, ruling out the possibility that the change in cell performance is due to a change in the electronic conductivity of the vanadate phase or the formation of an insulating layer at the YSZ-vanadate interface.

In situ characterization of the phase composition and structure of the $Ce_{0.8}Sr_{0.1}Cu_{0.05}Co_{0.05}VO_3$-YSZ composite anode in both the high- and low-activity states, in the region near the electrolyte-anode interface, would be required to provide a definitive explanation for the observed hysteresis in electrochemical properties. However, the results here provide important clues as to its possible origin. It is useful to first consider the structure of the Cu and Co nanoparticles that are exsolved from the $Ce_{0.8}Sr_{0.1}Cu_{0.05}Co_{0.05}VO_3$ lattice under reducing conditions. The hydrocarbon stability tests (Figure 3) demonstrate that the anode has relatively low catalytic activity for the production of carbon fibers from hydrocarbons. Since Co by itself has high activity for this reaction, Co nanoparticles must be in intimate contact with Cu

on the reduced electrode. Since Cu and Co are nearly immiscible and do not form bulk alloys, the nanoscale mixtures of these metals that are produced by the exsolution process would be expected to phase separate; furthermore, due to the lower surface free energy of Cu, one would expect this process to produce Cu-coated Co particles.

A previous study of a Cu-CeO_2-YSZ composite electrode (the Cu and CeO_2 were added using wet infiltration) that was coated with a thin layer of Co using electrodeposition demonstrated that Cu does indeed segregate to a Co surface.[51] Under typical SOFC operating conditions, this anode was found to have high hydrocarbon stability and did not catalyze carbon fiber formation. In this study X-ray photoelectron spectroscopy (XPS) was used to characterize a 250-nm Co film that had been electrodeposited onto a Cu foil as a function of temperature in ultra-high vacuum (a reducing environment). It was found that, at temperatures above 800 K, Cu migrated through the Co film, ultimately coating its surface. Furthermore, analysis of the XPS peak intensities during sputter depth-profile measurements indicated that the equilibrium thickness of the Cu coating was only 1-2 monolayers. Applying these results to the reduced $Ce_{0.8}Sr_{0.1}Cu_{0.05}Co_{0.05}VO_3$ electrode used in the present study, the exsolved Co nanoparticles will also become coated with a 1-2 monolayers of Cu.

While coating of the Co particles with a thin layer of Cu could explain the low activity of the reduced $Ce_{0.8}Sr_{0.1}Cu_{0.05}Co_{0.05}VO_3$ anode for carbon deposition, some Co must still be exposed since the catalytic activity of the anode for H$_2$ oxidation at high cell potentials is essentially the same as that for an electrode that contains only Co nanoparticles. Based on these observations, we propose that, for the $Ce_{0.8}Sr_{0.1}Cu_{0.05}Co_{0.05}VO_3$ anode, some Co is present in the thin Cu layer that coats the Co nanoparticles, as shown schematically in Figure 5. Note that the mechanism for transition metal catalyzed formation of carbon fibers from hydrocarbons involves the dissolution of carbon into the metal and the precipitation of a metal carbide particle that is lifted off the surface of the original metal particle by the growing carbon fiber.[5,61] This process would not occur for the isolated Co atoms in the surface Cu layer shown in Figure 5, but these atoms would be expected to retain their catalytic activity for oxidation reactions.

It is interesting to estimate the anode overpotentials corresponding to the critical points in the V-i curve for the cell with the $Ce_{0.8}Sr_{0.1}Cu_{0.05}Co_{0.05}VO_3$ anode. Based on the estimated anode ASR for the high- and low-activity regions of curve (0.15 Ω cm^2 and 0.65 Ω cm^2), the anode overpotentials at the points where the performance jumps occur are 0.165 V (0.15 Ω cm$^2 \cdot$ 1.1 Acm^{-2}) and 0.163 V (0.65 Ω cm$^2 \cdot$ 0.25 Acm^{-2}), respectively. This in turn can be related to an increase in the P_{O2} in the three-phase boundary (TPB) region relative to the anode compartment gas phase, from 10^{-24} atm in the anode compartment to approximately 10^{-20} atm at the TPB.

Although the P_{O2} at the TPB remains well below that needed to oxidize either bulk Co (~10^{-18} atm[62]) or Cu (~10^{-11} atm[63]), we suggest that the switch in catalytic performance of the $Ce_{0.8}Sr_{0.1}Cu_{0.05}Co_{0.05}VO_3$-YSZ anode from that characteristic of a Co catalyst to one characteristic of a Cu catalyst at low cell potentials is due to oxidation of the Co that is exposed in the Cu-coated, Co
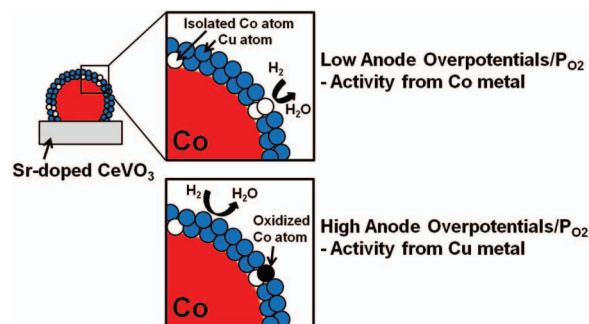
Figure 5. Schematic of the structure of the Cu-Co particles and the effect of polarization.

particles on the electrode surface. It would not be surprising if these isolated cobalt atoms have thermodynamic properties that vary somewhat from that of the bulk material. Indeed, it has been suggested that small Co nanoparticles are more easily oxidized than bulk Co and can become oxidized at a significantly lower P_{O2}.[62,63] Support and promoter effects have also been reported to alter the redox properties of small Co particles.[62] Since CoO does not exhibit the high oxidation activity of metallic Co, when the Co becomes oxidized the catalytic activity would decrease. The observed switching behavior for the Cu-Co system is therefore likely to be due to oxidation/reduction of the surface Co in the Cu-Co particles at the P_{O2} corresponding to an anode overpotential of ∼0.164 V. Based on this scenario, the exposed Co provides the catalytic activity at low anode overpotentials (low P_{O2}) and Cu provides the catalytic activity at high overpotentials as shown schematically in Figure 5.

The performance of the anodes made with Cu-Co mixtures is very intriguing and provides another example of the use of exsolution from an oxide host under reducing conditions as an in situ means to synthesize catalytic metal nanoparticles on SOFC electrode surfaces and also shows how the anode overpotential and the local P_{O2} can affect the structure and catalytic properties of bimetallic metal catalyst particles. Since $Ce_{0.8}Sr_{0.1}Cu_{0.05}Co_{0.05}VO_3$-YSZ composite anodes appear to be hydrocarbon tolerant and exhibit good performance at low overpotentials in H_2 fuel these materials hold some promise for use in SOFC. The performance and stability of these anodes while operating with hydrocarbon fuels, and whether similar hysteresis phenomena occur with hydrocarbons, will be the subject of a future study.

Conclusions

In this study it was demonstrated that upon reduction in humidified hydrogen at 973 K zircon-type $Ce_{0.8}Sr_{0.1}Cu_{0.05}TM_{0.05}VO_{4-0.5x}$ oxides (TM = Ni or Co) undergo a phase transition to the perovskite structure which is accompanied by exsolution of a portion of the transition metals from the lattice. The exsolved metals form Cu-Ni and Cu-Co mixtures with the surface of the mixture enriched with Cu due to its lower surface energy (note that Ni and Cu form an alloy, while Co and Cu form separate phases), which decorate the surface of the oxide. The hydrocarbon stability tests and the electrochemical performance measurement demonstrated that majority of the Co nanoparticles must be at least partially coated with the Cu, with some isolated Co atoms in the surface Cu layer providing the catalytic activity for H_2 oxidation. However, an unusually complex behavior was exhibited by the cell with the $Ce_{0.8}Sr_{0.1}Cu_{0.05}Co_{0.05}VO_3$-YSZ composite anode including hysteresis in the polarization curve with abrupt changes in performance occurring at several voltages. The switch in the performance of the $Ce_{0.8}Sr_{0.1}Cu_{0.05}Co_{0.05}VO_3$-YSZ anode from that characteristic of one with a Co catalyst to one with a Cu catalyst at low cell voltages indicates that the isolated cobalt sites are being oxidized at higher anode overpotentials.

Acknowledgment

References

1. R. J. Gorte, J. S. Kim, V. V. Nair, and J. M. Vohs, *Scripta Mater*, **65**, 90 (2011).
2. R. J. Gorte, S. Park, J. M. Vohs, and C. H. Wang, *Adv Mater*, **12**, 1465 (2000).
3. R. J. Gorte, J. M. Vohs, and S. McIntosh, *Solid State Ionics*, **175**, 1 (2004).
4. S. McIntosh and R. J. Gorte, *Chem Rev*, **104**, 4845 (2004).
5. M. L. Toebes, J. H. Bitter, A. J. van Dillen, and K. P. de Jong, *Catal Today*, **76**, 33 (2002).
6. M. D. Gross, K. M. Carver, M. A. Deighan, A. Schenkel, B. M. Smith, and A. Z. Yee, *J Electrochem Soc*, **156**, B540 (2009).
7. G. Kim, M. D. Gross, W. Wang, J. M. Vohs, and R. J. Gorte, *J Electrochem Soc*, **155**, B360 (2008).
8. S. Lee, G. Kim, J. M. Vohs, and R. J. Gorte, *J Electrochem Soc*, **155**, B1179 (2008).
9. D. Neagu and J. T. S. Irvine, *Chem Mater*, **22**, 5042 (2010).
10. A. Vincent, J. L. Luo, K. T. Chuang, and A. R. Sanger, *J Power Sources*, **195**, 769 (2010).
11. A. Babaei, L. Zhang, S. L. Tan, and S. P. Jiang, *Solid State Ionics*, **181**, 1221 (2010).
12. G. Kim, G. Corre, J. T. S. Irvine, J. M. Vohs, and R. J. Gorte, *Electrochem Solid St*, **11**, B16 (2008).
13. M. van den Bossche, R. Matthews, A. Lichtenberger, and S. McIntosh, *J Electrochem Soc*, **157**, B392 (2010).
14. X. B. Zhu, Z. Lu, B. Wei, M. L. Liu, X. Q. Huang, and W. H. Su, *Electrochim Acta*, **55**, 3932 (2010).
15. D. M. Bierschenk, E. Potter-Nelson, C. Hoel, Y. G. Liao, L. Marks, K. R. Poeppelmeier, and S. A. Barnett, *J Power Sources*, **196**, 3089 (2011).
16. L. Adijanto, R. Kungas, J. Park, J. M. Vohs, and R. J. Gorte, *Int J Hydrogen Energ*, **36**, 15722 (2011).
17. B. H. Smith and M. D. Gross, *Electrochem Solid St*, **14**, B1 (2011).
18. C. H. Toh, P. R. Munroe, D. J. Young, and K. Foger, *Mater High Temp*, **20**, 129 (2003).
19. H. Kim, C. Lu, W. L. Worrell, J. M. Vohs, and R. J. Gorte, *J Electrochem Soc*, **149**, A247 (2002).
20. Y. Matsuzaki and I. Yasuda, *Solid State Ionics*, **132**, 261 (2000).
21. D. Sarantaridis and A. Atkinson, *Fuel Cells*, **7**, 246 (2007).
22. G. Kim, S. Lee, J. Y. Shin, G. Corre, J. T. S. Irvine, J. M. Vohs, and R. J. Gorte, *Electrochem Solid St*, **12**, B48 (2009).
23. W. Kobsiriphat, B. D. Madsen, Y. Wang, L. D. Marks, and S. A. Barnett, *Solid State Ionics*, **180**, 257 (2009).
24. J. S. Kim, V. V. Nair, J. M. Vohs, and R. J. Gorte, *Scripta Mater*, **65**, 90 (2011).
25. Z. H. Bi and J. H. Zhu, *J Electrochem Soc*, **158**, B605 (2011).
26. M. D. Gross, J. M. Vohs, and R. J. Gorte, *J Electrochem Soc*, **154**, B694 (2007).
27. G. L. Xiao, C. Jin, Q. Liu, A. Heyden, and F. L. Chen, *J Power Sources*, **201**, 43 (2012).
28. Y. Wang, B. D. Madsen, W. Kobsiriphat, S. A. Barnett, and L. D. Marks, *Microsc Microanal*, **13**, 100 (2007).
29. B. D. Madsen, W. Kobsiriphat, Y. Wang, L. D. Marks, and S. A. Barnett, *J Power Sources*, **166**, 64 (2007).
30. L. Adijanto, V. B. Padmanabhan, R. Kungas, R. J. Gorte, and J. M. Vohs, *J Mater Chem*, **22**, 11396 (2012).
31. W. Kobsiriphat, B. D. Madsen, Y. Wang, M. Shah, L. D. Marks, and S. A. Barnett, *J Electrochem Soc*, **157**, B279 (2010).
32. J. A. Kurzman, J. Li, T. D. Schladt, C. R. Parra, X. Y. Ouyang, R. Davis, J. T. Miller, S. L. Scott, and R. Seshadri, *Inorg Chem*, **50**, 8073 (2011).
33. Y. Nishihata, J. Mizuki, T. Akao, H. Tanaka, M. Uenishi, M. Kimura, T. Okamoto, and N. Hamada, *Nature*, **418**, 164 (2002).
34. U. G. Singh, J. Li, J. W. Bennett, A. M. Rappe, R. Seshadri, and S. L. Scott, *J Catal*, **249**, 349 (2007).
35. I. Tan, M. Taniguchi, H. Tanaka, M. Uenishi, N. Kajita, Y. Nishihata, J. Mizuki, and K. Niihara, *Key Engineering Materials*, **317–318**, 833 (2006).
36. H. Tanaka, M. Taniguchi, M. Uenishi, N. Kajita, I. Tan, Y. Nishihata, J. Mizuki, K. Narita, M. Kimura, and K. Kaneko, *Angew Chem Int Edit*, **45**, 5998 (2006).
37. H. Tanaka, M. Uenishi, M. Taniguchi, I. Tan, K. Narita, M. Kimura, K. Kaneko, Y. Nishihata, and J. Mizuki, *Catal Today*, **117**, 321 (2006).
38. Z. Cheng, S. W. Zha, L. Aguilar, and M. L. Liu, *Solid State Ionics*, **176**, 1921 (2005).
39. M. Cooper, K. Channa, R. De Silva, and D. J. Bayless, *J Electrochem Soc*, **157**, B1713 (2010).
40. N. Danilovic, J. L. Luo, K. T. Chuang, and A. R. Sanger, *J Power Sources*, **192**, 247 (2009).
41. J. S. Park, I. D. Hasson, M. D. Gross, C. Chen, J. M. Vohs, and R. J. Gorte, *J Power Sources*, **196**, 7488 (2011).
42. C. Peng, J. L. Luo, A. R. Sanger, and K. T. Chuang, *Chem Mater*, **22**, 1032 (2010).
43. C. T. G. Petit, R. Lan, P. I. Cowin, J. T. S. Irvine, and S. W. Tao, *J Mater Chem*, **21**, 525 (2011).
44. C. T. G. Petit, R. Lan, P. I. Cowin, A. Kraft, and S. W. Tao, *J Mater Sci*, **46**, 316 (2011).
45. E. V. Tsipis, V. V. Kharton, N. P. Vyshatko, A. L. Shaula, and J. R. Frade, *J Solid State Chem*, **176**, 47 (2003).
46. A. Watanabe, *J Solid State Chem*, **153**, 174 (2000).
47. L. Adijanto, V. B. Padmanabhan, K. J. Holmes, R. J. Gorte, and J. M. Vohs, *J Solid State Chem*, **190**, 12 (2012).
48. M. D. Gross, J. M. Vohs, and R. J. Gorte, *J Mater Chem*, **17**, 3071 (2007).
49. M. D. Gross, J. M. Vohs, and R. J. Gorte, *Electrochim Acta*, **52**, 1951 (2007).
50. S. W. Jung, J. M. Vohs, and R. J. Gorte, *J Electrochem Soc*, **154**, B1270 (2007).
51. S. Jung, M. D. Gross, R. J. Gorte, and J. M. Vohs, *J Electrochem Soc*, **153**, A1539 (2006).
52. S. I. Lee, K. Ahn, J. M. Vohs, and R. J. Gorte, *Electrochem Solid St*, **8**, A48 (2005).
53. S. I. Lee, J. M. Vohs, and R. J. Gorte, *J Electrochem Soc*, **151**, A1319 (2004).
54. S. Park, R. J. Gorte, and J. M. Vohs, *J Electrochem Soc*, **148**, A443 (2001).
55. R. Kungas, J. S. Kim, J. M. Vohs, and R. J. Gorte, *J Am Ceram Soc*, **94**, 2220 (2011).
56. W. S. Wang, M. D. Gross, J. M. Vohs, and R. J. Gorte, *J Electrochem Soc*, **154**, B439 (2007).
57. J. M. Vohs and R. J. Gorte, *Adv Mater*, **21**, 943 (2009).

58. L. Adijanto, R. Kungas, F. Bidrawn, R. J. Gorte, and J. M. Vohs, *J Power Sources*, **196**, 5797 (2011).
59. K. B. K. Teo, C. Singh, M. Chhowalla, and W. I. Milne, *Encyclopedia of Nanoscience and Nanotechnology*, edited by H. S. Nalwa, Vol. X, pp. 1–22 (2003).
60. K. Bakhmutsky, N. L. Wieder, T. Baldassare, M. A. Smith, and R. J. Gorte, *Appl Catal a-Gen*, **397**, 266 (2011).
61. P. R. Shah, T. Kim, G. Zhou, P. Fornasiero, and R. J. Gorte, *Chem Mater*, **18**, 5363 (2006).
62. A. Navrotsky, C. C. Ma, K. Lilova, and N. Birkner, *Science*, **330**, 199 (2010).
63. E. van Steen, M. Claeys, M. E. Dry, J. van de Loosdrecht, E. L. Viljoen, and J. L. Visagie, *J Phys Chem B*, **109**, 3575 (2005).